Nano Energy 50 (2018) 504–512

Contents lists available at ScienceDirect

Nano Energy

journal homepage: www.elsevier.com/locate/nanoen

Communication

Assessment of extracellular matrix modulation of cell traction force by using silicon nanowire array

Hongqing Feng[a,b,c,1], Han Ouyang[a,b,1], Mingzeng Peng[a,b,1], Yiming Jin[a,b], Yalan Zhang[a,b], Zhuo Liu[a,d], Yang Zou[a,b], Chaochao Zhao[a,b], Yubo Fan[d], Junyi Zhai[a,b,c,*], Zhong Lin Wang[a,b,c,e,*], Zhou Li[a,b,c,*]

[a] CAS Center for Excellence in Nanoscience, Beijing Key Laboratory of Micro-nano Energy and Sensor, Beijing Institute of Nanoenergy and Nanosystems, Chinese Academy of Sciences, Beijing 100083, PR China
[b] School of Nanoscience and Technology, University of Chinese Academy of Sciences, Beijing 100049, PR China
[c] Center on Nanoenergy Research, School of Physical Science and Technology, Guangxi University, Nanning 530004, China
[d] School of Biological Science and Medical Engineering, Beihang University, Beijing 100191, China
[e] School of Materials Science and Engineering, Georgia Institute of Technology, Atlanta, GA 30332-0245, United States

ARTICLE INFO

Keywords:
Cell traction force
Focal adhesion
Si nanowires array
Extracellular matrix
Focal adhesion

ABSTRACT

Extracellular matrix (ECM) has critical influence on cell adhesion and force generation, and has been wildly used in tissue engineering scaffolds to promote cell growth and function. A uniform, precise and densified silicon nanowires (Si-NW) array was fabricated to investigate the dynamics of cell traction force (CTF) modulated by ECM at submicron spatial resolution. The CTF result suggested that the time slot from 6 h to 24 h was critical for fibronectin to enhance CTF generation. Fibronectin also increased the formation of the cellular membrane-bound focal adhesion (FA), and the enhancement pattern of CTF and FA due to fibronectin modulation were highly similar. Meanwhile, the trends of CTF and FA dynamics in either the fibronectin modified or the bare Si-NW array were coordinated with each other, respectively. These results identified that the consistency of FA formation and CTF generation lasted for as long as dozens of hours. In addition, the effective modulation slot of the external ECM was within 36 h, revealing the existence of a balanced time point for the self-secreted ECM to pull up with the externally added ECM after the cells started to grow on the scaffolds. The influence of data sampling on CTF measurement was also evaluated. This investigation provides important information for the understanding of the CTF derivation dynamics and the design of ECM modified tissue engineering scaffolds.

1. Introduction

Biomedical scaffolds and implants have been widely applied in research and clinical fields. To guarantee their proper function in the body, adequate cell adhesion to the scaffold and implants is vitally important. Extracellular matrix (ECM) plays a critical role in cell adhesion, development and functionality. ECM not only serves as the substrate for cell anchorage, but also provides suitable physical microenvironment for the cells to grow and play their functions [1,2]. The structure, elasticity, chemical composition and mechanical properties have all been reported to enhance the cell survival, growth, sensing, response, and communication with the substrate and neighboring cells [3,4]. Fibronectin is a major component of ECM and extensively expressed by multiple cell types, mediating a wide variety of cellular interactions with the ECM [5]. It has been found to be very effective in enhancing the cell adhesion and regeneration on the artificial matrix or implants in vitro or in vivo for biomedical engineering purposes [6]. Gradually it is routine to modify the artificial scaffolds or matrices with fibronectin to enhance cell adhesion and promote cell development in biomedical applications [7].

Cells adhere to the ECM via focal adhesion (FA), the specialized sites on the cell membrane at the end of intracellular bundled and cross-linked actin stress fiber networks [8,9]. At the site of FA, integrins cluster into supramolecular complexes with structural proteins including talin, vinculin, and paxillin (Fig. 1). These proteins form the structures of FA, which have diverse functional connections with cell sensing of the environment and the cellular signal pathways [10]. Upon adhesion to the ECM, cells will generate cell traction force (CTF) via

* Corresponding authors at: CAS Center for Excellence in Nanoscience, Beijing Key Laboratory of Micro-nano Energy and Sensor, Beijing Institute of Nanoenergy and Nanosystems, Chinese Academy of Sciences, Beijing 100083, PR China.
E-mail addresses: jyzhai@binn.cas.cn (J. Zhai), zlwang@gatech.edu (Z.L. Wang), zli@binn.cas.cn (Z. Li).
[1] These authors contributed equally to this work.

https://doi.org/10.1016/j.nanoen.2018.05.057
Received 24 April 2018; Received in revised form 14 May 2018; Accepted 21 May 2018
Available online 24 May 2018

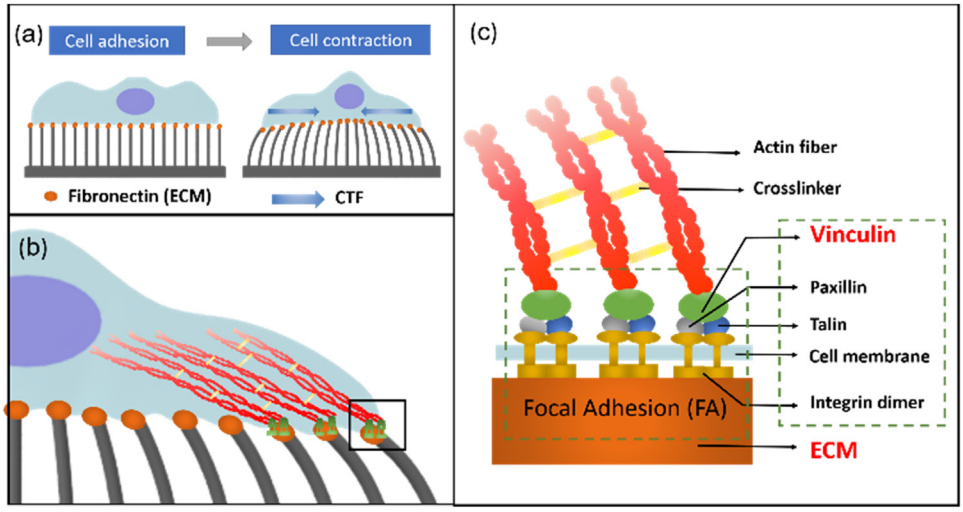

Fig. 1. The study of ECM modulation effect on CTF and FA. (a) MC-3T3 cells adhere to the highly ordered and dense Si-NW array substrate, and the Si-NW bent due to the CTF generated by the MC-3T3 cells. (b) The formation of FA and crosslinked actin stress fibers on ECM modified substrate. (c) The detailed information of FA and actin fibers.

contraction of the actin cytoskeleton and transmit this force via FA to the underlying substrate [11]. The change of CTF can regulate the cytoskeleton structure, activate multiple signalling pathways and determine the fate of cells in vitro [12]. It has been shown that FA are stimulated to grow after the application of a local external force [13]. It's also reported that the force applied at FA determined their assembly via actomyosin contraction on a time scale below seconds. The force direction correlated with the main axis of the FA's elongation, and the measured forces were linearly related to the total fluorescence intensity of GFP–vinculin [14]. Recently, Sarangi et al. found that the FA internal forces at molecular scales coordinated with the CTF exerted at the cell-substrate interface to regulate FA organization and dynamics [15]. ECM stiffness can modulate FA sensing to guide durotaxis through a specific pathway downstream of FAK [16,17]. ECM ligands and rigidity not only impact cell-ECM traction but also alters cell–cell tension [18]. On the other hand, CTF can induce the unfold of fibronectin in the ECM of living cells to alter outside-in cell signalling [19], or induce fibrillogenesis and guide the direction of developing fibril [20].

In conclusion of the above mentioned reports, there exists complicated crosstalk among ECM, CTF and FA. However, the mechanisms are still not fully elaborated. One of the most important reason is the inconvenience to do cell force measurement. The conventional technologies capable to do cell force measurement include atomic force microscopy, optical tweezers, micropipettes, and flow chambers [21–25]. Benoit and Wang et al. respectively designed mechanically and genetically combined approach to measure the single molecular forces which were at pico-Newton level [26,27]. Nevertheless the most prevalently employed CTF measurement approaches have been the polydimethylsiloxane (PDMS) films containing fluorescent beads or PDMS microposts / micropillars / microcolumns with or without fluorescently marked tops [28–36]. Meanwhile, ordered inorganic nanowire array have also been developed because they have better resolution [37–39]. Silicon (Si), which has good biocompatibility, is an optimal candidate. The fabrication technologies of Si nanostructures have been well developed [40–42]. Silicon nanowire (Si-NW) have been demonstrated as unique probes for quantifying biological processes at a high spatial resolution [43,44]. In addition, the high Young's modulus and aspect ratio of Si-NW guarantee their bending without stretching under lateral force. Therefore, the obtained results were precise and reliable. By measurement on Si-NW, HeLa and L929 cancer cells were found to have significantly larger CTF than normal cells, and they were all at micro-Newton level [45]. Recently, Sahoo et al. developed a InP NWs array to investigate the enhanced adhesion of single bacterium after biofilm formation [46]. Also, Adolfsson et al. developed fluorescent GaP-GaInP NWs heterostructures that could precisely determine the NWs position with respect to cells [47]; Hallstrom et al. employed GaP NWs array to measure the contraction of the neural growth cones [48]. Each method has specific advantages and disadvantages. To understand further the mechanisms underlying the crosstalk of ECM, CTF and FA, deeper explorations are still necessary.

In this work, we studied the influence of ECM on CTF and FA at submicron level by directly culturing osteoblast MC-3T3 cells on the Si-NW array substrate with or without fibronectin modification. Well-aligned and uniform Si-NW array with high-density and accuracy was fabricated for direct cell culture (Fig. 1). The CTF were characterized by measuring the content of NW bending due to the pull of the cells in the culture process at 2 h, 6 h, 12 h, 24 h, and 36 h, respectively. The CTF measured from the fibronectin modified Si-NW array were significantly higher than those measured from bare Si-NW array from 6 h to 24 h. Fibronectin also increased the formation of FA. The enhancement pattern of CTF induced by fibronectin was in accordance with that of FA in the entire 36 h culture. Meanwhile, the trends of CTF and FA dynamics in either the fibronectin modified or the bare Si-NW array were also coordinated with each other, respectively. The influence of data sampling on CTF measurement was also evaluated. This study provided valuable information for the understanding of the CTF derivation dynamics and the design of ECM modified tissue engineering scaffold.

2. Experimental section

2.1. The fabrication of the Si-NW array

The fabrication process was schematically shown in Fig. S1. First a layer of photoresist was deposited on the Si wafer, then ordered pits array were made on the photoresist by electron beam lithography (EBL). The diameter of the pits was set to be 250 nm, and the spaces in between to be 700 nm. Then a layer of Ni film with 100 nm thickness was deposited on the wafer. After the photoresist was removed and the metal film was lift-off, the wafer was left with array of Ni nano-cylinders. The Ni nano-cylinders worked as etching masks in the following Bosch process to produce Si-NW array. Finally, the remnant Ni metal was removed by sulfuric acid, hydrogen peroxide, and deionized water mixed solution.

2.2. The culture of MC-3T3 cells on the Si-NW array

MC-3T3 osteoblasts were cultured on the bare and fibronectin-modified Si-NW array for CTF measurement in these two different conditions. The wafer with aligned Si-NW array was cut into small pieces and put in 96 well plates. They were sterilized by immergence in 75% medical standard ethanol for 2 h and then exposed to a high-dose UV light for 2 h. After sterilization, the pieces with aligned Si-NW array

were rinsed by deionized water (DI water) 3 times. Then the Si-NW were immersed in the fibronectin solution (human fibronectin, 50 μg/mL in deionized water; Sigma-Aldrich Co. LLC Natick, MA 0176, USA) for 12 h, and then rinsed by PBS for 3 times. This made the fibronectin-modified Si-NW. The bare Si-NW were immersed in PBS for 12 h before use. MC-3T3 cells were seeded into the 96 well plate at a density of 3000 cells per well. After culture, the Si-NW samples were taken out of cell culture medium and the cells attached on them were fixed with 4% paraformaldehyde (in 1 × PBS) for 2 h and then further rinsed three times with PBS buffer. They were further immersed in 1% chlorauric acid (in DI water) for 2 h for contrast enhancement. Then the cells were dehydrated in a series of ethanol solutions (25, 50, 75, 90, 95, and 100 v/v %) for 5 min each sequentially, and observed under SEM.

2.3. The measurement of CTF using the Si-NW array

The displacement of each single NW tip from its original position was measured from the top-view SEM image using software Image-Pro Plus 6.0, and the displacements were used to derive the CTF parallel to the substrate (Fig. S2). Finite Element (FEM) simulations were carried out to derive the relationship between the tIp displacement and the corresponding applied CTF. The FEM simulation was based on COMSOL package including nonlinear mechanical effects. The shape of the Si-NW was modelled as a pole with a diameter of 267 nm and length of 3315 nm, in accordance with the SEM characterizations. The mechanical properties for silicon were set as follows: Young's modulus $E = 150$ GPa [45], Poisson's ratio = 0.278, and the density $\rho = 2330\ kg/m^3$. The calculated curve was shown in Fig. S2. In a large displacement range, a linear fit worked well for CTF calculation: CTF (μN) = 4.13 (μN/nm) × displacement (nm). Throughout our experiment, the displacements of the NWs tips were within the linear range, therefore the CTF were derived using the above equation in this study.

2.4. Immune-fluorescent staining of the FA

The FA was stained with mouse anti-mouse vinculin primary antibody, and then with the green fluorescent donkey anti-mouse IgG secondary antibody. The defined bright green dots or bunches represented the formation of FA. The cytoskeleton F-actin were stained red with Alexa Fluor® 568 Phalloidin, and the nucleus were stained blue with DAPI.

2.5. Statistical analysis

The CTF measured in each group was shown as Average ± SE in the plots. The p-value was calculated using two tailed T-test.

3. Results and discussion

3.1. The Si-NW array for cell culture and CTF measurement

The fabricated dense and uniform Si-NW array is shown in Fig. 2a-d. The diameter of the NW was measured to be 267 ± 9 nm; the space between the centers of each NW was 687 ± 23 nm; and the length of the NW was 3315 ± 24 nm (n = 30). The extremely small variance in the diameter and height of the NW ensured a defined and precise measurement of the CTF. In addition, the density of the Si-NW array reached 4 NW per μm^2 (Fig. 2b). The cells adhere and grew well on top of the Si-NW array, spreading into spindle-like shapes at 12 h (Fig. 2e). The cells grew on top of the Si-NW array, showing no deformation or sinking into the bottom of the NW, or penetration by the NW; some NW underneath the cell margin was bent by the CTF (Fig. 2f). Very occasionally some part of the cellular skeleton structure collapsed at the cell margin area, and these parts were excluded from CTF measurement (Fig. S1b).

This fabricated array is highly beneficial for cell growth and CTF measurement. In previous studies whereas the diameters of the NW was less than 100 nm or with sharp tips [49], the cells were often found to be penetrated [50] or deformed down to the bottom of the NW [51], causing holes or membrane folds in the cells [52,53]. These may impair cell division, reduce cell motility or cause irregular nuclei. In our NW array, however, the diameter of the NW was averagely 267 nm, and the tops of the NW were flat. These features supported the cell growth much better, because a large flat substrate made better anchor for the cells and produced less stress to them. In addition, the NW density was up to 4 NW per μm^2. It's been reported that cells represented much less irregular nuclei on the 4 NW per μm^2 array than those with a lower density [54]. Therefore our Si-NW array brings in many advantages for cell culture and CTF measurement.

3.2. MC-3T3 CTF measurement on the Si-NW array

The SEM images of the osteoblasts cultured on the bare Si-NW array (control) and fibronectin-modified (Fn) Si-NW array for 6 h were shown in Fig. 3a-b. The displacements of the Si-NW tops in the fibronectin group were evidently larger than those in control group. Because no difference between the control and experimental group existed other than the presence of fibronectin, it directly demonstrated that the exerted CTF were stronger at the presence of fibronectin. A linear fit was obtained for CTF calculation: CTF (μN) = 4.13 (μN/nm) × displacement (nm), which worked well throughout our experiment. Fig. 3c showed the modelled force field and the spatial distribution of the CTF of a single MC-3T3 cells. The distance between the CTF vectors was as short as about 700 nm, achieving the submicron level. This Si-NW array enabled measurement with high-resolution, which is demanded for CTF measurement [29].

3.3. The dynamics of CTF in 36 h on the bare and fibronectin-modified Si-NW array

The CTF of the MC-3T3 cells in the 36 h culture were measured and recorded. There were 15 ~ 24 cells analysed for each group at each time point. For each cell, 3 ~ 41 NWs were measured for their tip displacement and calculated for the corresponding CTF. Totally there were 180 ~ 518 NWs measured in each group. Fig. 4a-1 was the time dependent CTF line plot of the fibronectin and control group (Average ± SE), and Fig. 4a-2 was the boxplot, with the p-value of two-tailed *t*-test of each pair marked on. At 2 h after seeding the cells, the CTF on the bare control Si-NW were the same as those on the fibronectin-modified ones. At 6 h, the CTF became greatly larger on the fibronectin-modified Si-NW. At 12 h, the significant difference was sustained. However, at 24 h, the CTF on the fibronectin-modified Si-NW became significantly smaller than on the control. Finally at 36 h, the CTF on the two groups became the same again. The average CTF of each group were in a range from 2.08 ± 0.03 μN to 2.71 ± 0.03 μN.

In Fig. 4a, up to 41 NWs derived CTF in a single cell were included for data analysed. This made the variance relatively large. We in further narrowed the range of data sampling, by allowing only the largest 5–8 CTF values for each cell in a certain group to make the total number of CTF in each group controlled within 102–120. As shown in Fig. 4b, the difference among the fibronectin and control group were kept the same except for the 24 h (marked with blue rectangles). The CTF in the fibronectin-modified group was still significantly smaller than the control group, but the probability that the CTF of the Fn group was not sufficiently smaller than that of the control group became larger, as indicated by the increased p values [55] (p value increased from 2.9×10^{-10} to 6.1×10^{-3}). The average CTF of each group were in a range from 2.50 ± 0.05 μN to 3.46 ± 0.05 μN. At last, we analysed only the largest 20 CTF in each group, as shown in Fig. 4c. The average CTF of each group were in a range from 3.29 ± 0.06 μN to 4.31 ± 0.07 μN. At this time, the CTF of the fibronectin-modified group became significantly higher than the control group

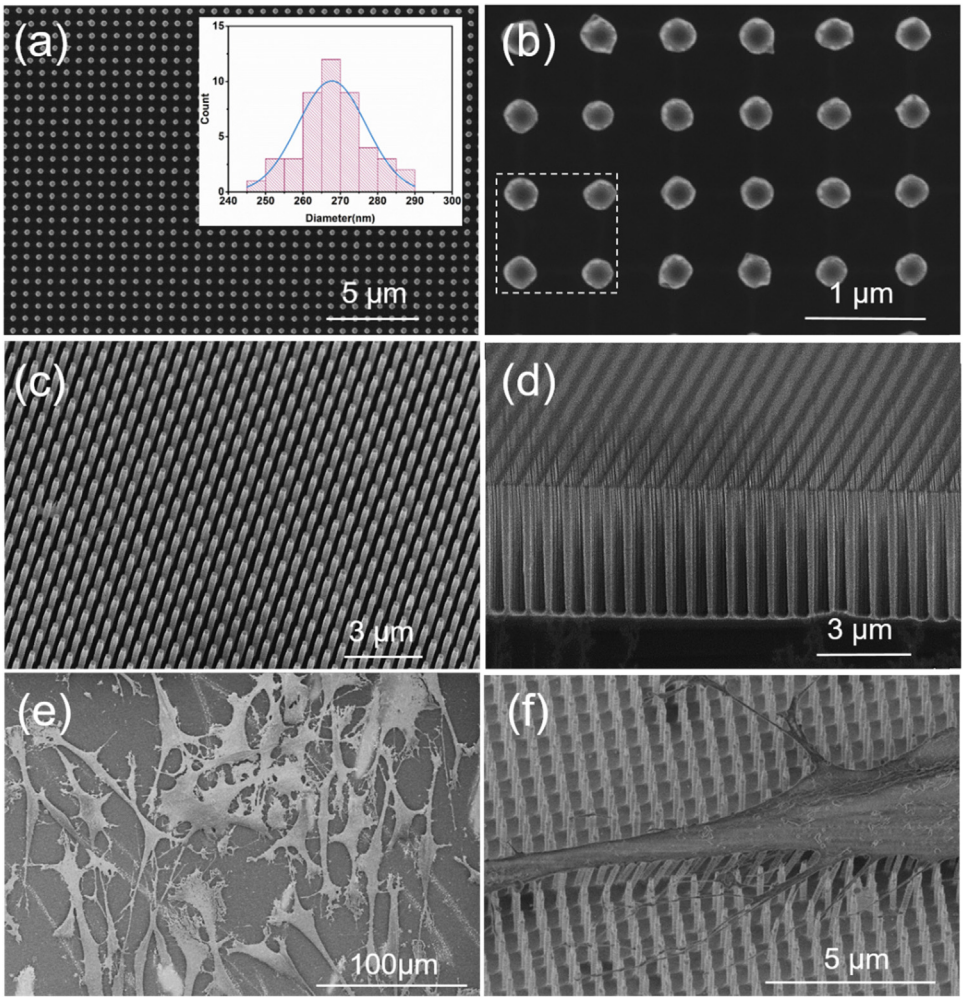

Fig. 2. (a) Top view of the Si-NW array for cell culture and CTF measurement. The inset of (a): the diameter of the NW was 267 ± 9 nm (n = 30). (b) The zoom-in top-view; the density of the array was 4 NW per μm^2. (c–d) The bird's eye-view and side-view, and the length of the NW was 3315 ± 24 nm (n = 30). (e) The cells spread and grew into spindle-like shapes at 12 h. The cells grew on top of the Si-NW array, showing no deformation or sinking into the bottom of the NW, or penetration by the NW. (f) Tilt 30 ° of the cells growing on the Si-NW array. Some NW underneath the cell margin were bent due to the CTF.

($p = 6.9 \times 10^{-4}$). The comparisons at other time points were still the same: there were no difference between the two groups at 2 h and 36 h; but at 6 h and 12 h, the CTF in fibronectin group was significantly larger than the control. The data variance become much smaller. From Fig. 4a to c, it's shown that the data sampling of the effective CTF (details were listed in Table S1) had important influence on the characteristics of the cells' mechanical property. At critical time points, the results may even be reversed by different data sampling. The distributions of the CTF were shown in Fig. S3. The influence of data sampling on the CTF distributions were the same as those on the CTF values.

3.4. The dynamics of FA in 36 h on the bare and fibronectin-modified substrate

The influence of fibronectin on the FA formation was also monitored. The immune fluorescent staining showed that cells on the fibronectin-modified substrate had more and larger FA than those on the bare substrate, and the area of the cell on the fibronectin-modified substrate were also obviously larger than the control (Fig. 5). The FA fluorescent images in the entire 36 h were recorded (Fig. S4), and the precise cell area, FA area and FA numbers of each cell were quantitatively measured using Image-Pro Plus 6.0. For each group at each time point, 15–30 cells were analysed. The trends of the cell area (Fig. S5), FA area and FA count (Fig. 5c-d) were very similar with each other. They were all significantly higher in the fibronectin group than the control group ($p < 0.05$). As the cells grew and expended their area during the process, the area and numbers of the FA in each cell increased accordingly. In this case, the measured area and number of the FA was normalized to the cell area for comparison between different time points. The trends of the FA area and FA number percentage were also very similar to each other (Fig. 5e–f). The FA area and number percentage of the fibronectin groups were significantly higher than those of the control groups at 6 h, 12 h, and 24 h ($p < 0.01$). But they were the same at 2 h and 36 h ($p > 0.05$). The p-values of each group were listed in Table S2.

3.5. The concordance of the CTF and FA in the 36 h: the dynamics

Fig. 5g-h showed the dynamics of CTF and FA area percentage together in the control and fibronectin-modified group, respectively (n = 20). The trends of the CTF and FA dynamics were consistent with each other in both groups. In the control group, the CTF went firstly downwards and then upwards, which gradually returned to the beginning level. It's the same case with FA area percentage (Fig. 5g). In the fibronectin group, the CTF went firstly upwards and then downwards, which also gradually returned to the beginning level. The FA area percentage went also in this trend (Fig. 5h). The data sampling of CTF didn't influence this corelation. With all the CTF data included, the CTF and FA dynamics were still quite concordant (Fig. S6). Previous studies have reported that the force applied at FA determined their assembly via actomyosin contraction on a time scale below seconds [14]. Here we discovered that the correlation between the CTF and FA lasted for as long as 36 h, going through every period of the cells, including adhesion, spreading, growth, proliferation, and mitosis.

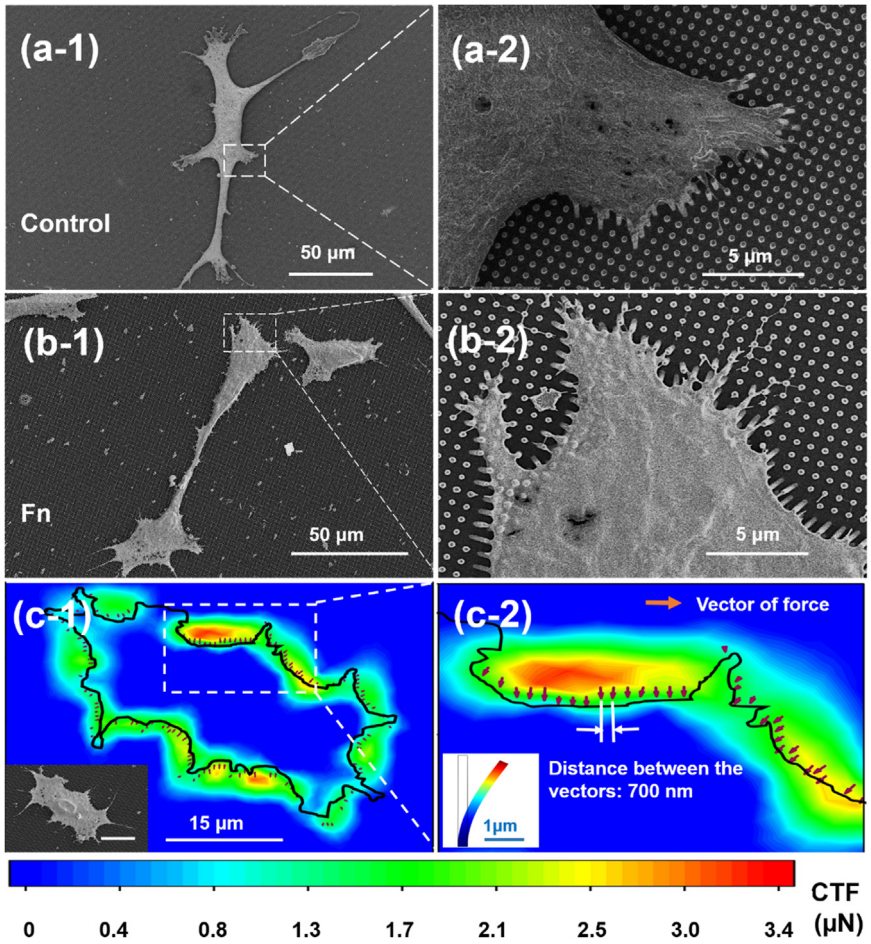

Fig. 3. The SEM images of osteoblast MC-3T3 cells on the bare (a) and fibronectin-modified (b) Si-NW after 6 h culture. (c) The modelled force field of a single MC-3T3 cell according to the displacement of the Si-NW tips. The inset of (c-1) was the SEM image of the cell (scale bar 15 μm), and the inset of (c-2) was the bending configuration of a single NW.

3.6. The concordance of the CTF and FA in the 36 h: the enhancement pattern

Comparing Fig. 4a-c with Fig. 5e-f, the enhancement pattern of the CTF and FA formation due to fibronectin modulation were also highly coordinated with each other (see also in Fig. S7). After the enhancement from 6 h to 24 h, the CTF in the fibronectin group finally returned to the same level as control at 36 h, which was the same situation as the beginning (2 h). The FA area percentage of the fibronectin group was also significantly higher than the control group in large part of the duration but was the same as control at the beginning (2 h) and the end (36 h). This enhancement pattern had a possible mechanism lying in the proliferation time of MC-3T3. The accurate growth curve of MC-3T3 cells was obtained by seeding 7.5×10^6 cells in 75 cm^2 culture plates at the same density of those growing on the Si-NW array in 96 well plate (3000 cells in 0.32 cm^2 wells). The cell numbers were counted at different time points, and the time for the cell number to double was found to be around 30 h, between 24 h and 36 h (Fig. S8). At the beginning, 2 h, there was no difference between fibronectin-modified and control group, because the cells had just started to adhere to the substrates, and had no response to the fibronectin as ECM. At 36 h, it's most probably that during a cycle of mitosis, the cells had expressed and secreted enough endogenous ECM to rival the exogenous supplied fibronectin. As the beginning of a new cycle, the FA and CTF started with a same level in the fibronectin-modified and control group. The growth curve was obtained with cells growing on the culture plate, therefore the double time may not be exactly the same as those on the NW array. However it can still be employed as a reference, because the NW array well supported the growth of the MC-3T3 cells.

3.7. The proper timeslot of ECM modification

In cell and tissue engineering field, the modification of the scaffolds with ECM is a routine procedure. However, ECM modification can produce both positive and negative roles for cell adhesion. For example, reduced cell extension or even induced apoptosis could be achieved by using micropatterned substrates with very small ECM islands (less than 10 μm^2 each) [56]. Therefore proper and precise ECM modification protocol may be more critical than normally considered. Here our findings indicated that the time slot for ECM existence was very important. If enhanced cell adhesion or modulation from the substrate is desired in long-term, for example longer than 36 h, additional ECM modification may be required.

3.8. The importance of data sampling for CTF measurement

The data sampling brought in some difference at 24 h for CTF measurement. With all CTF data included, the fibronectin group was significantly smaller than the control group at 24 h, which was not consistent with the FA percentage. If only the largest 20 CTF were included, the fibronectin group was significantly higher than control at 24 h, which was consistent with the FA percentage. Because previous studies have reported that the CTF stimulated the FA formation, and the CTF values correlated with the total fluorescence intensity and area of

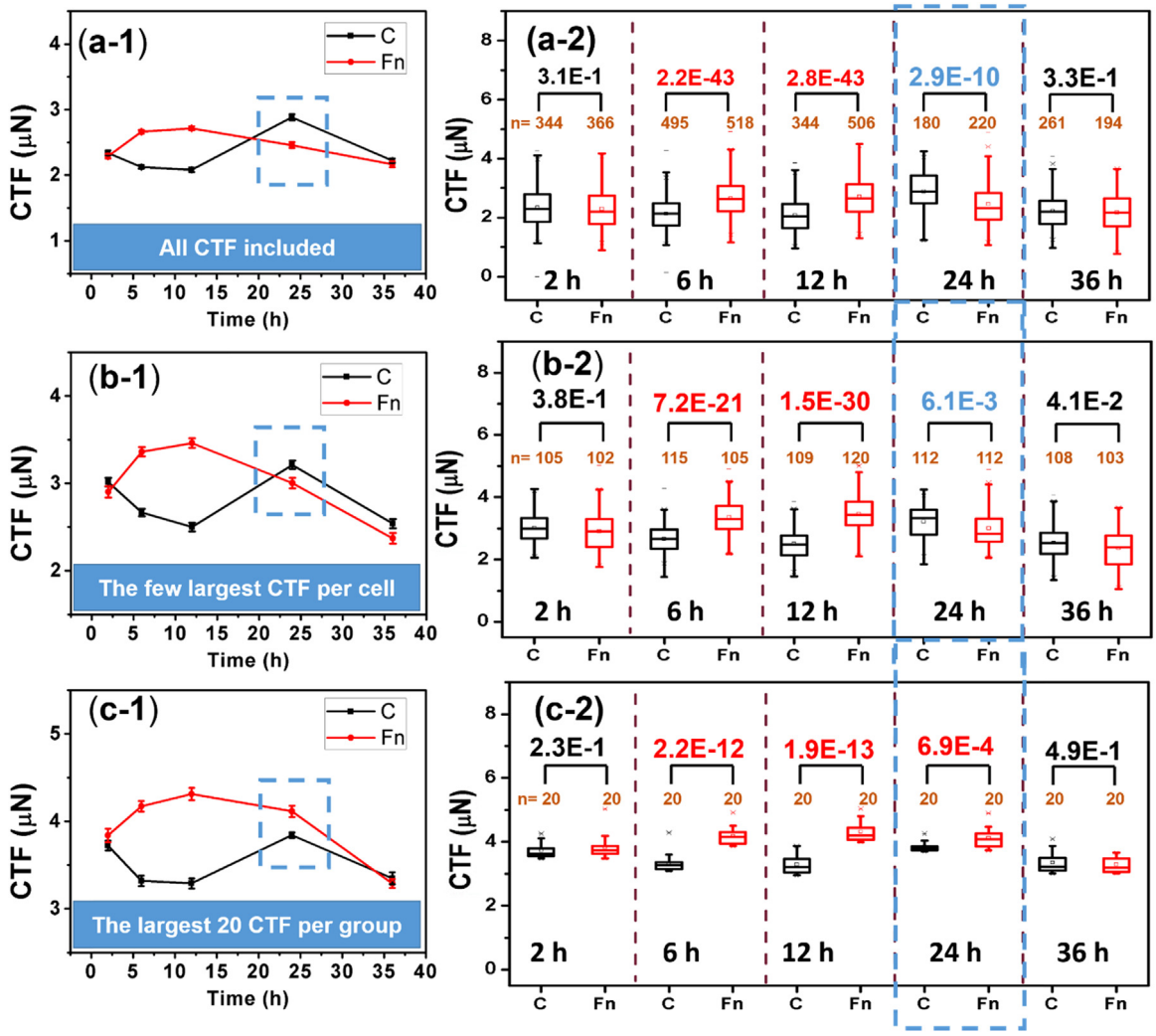

Fig. 4. (a) The line-plot and boxplot of the MC-3T3 CTF dynamics in 36 h on the control and fibronectin-modified Si-NW array, with all the measured CTF from single NW included (n = 180–506). (b) The line-plot and boxplot of the MC-3T3 CTF dynamics in 36 h on the control and fibronectin-modified Si-NW array, with only the 5–8 largest CTF from one cell included (n = 102–120). (c) The line-plot and boxplot of the MC-3T3 CTF dynamics in 36 h on the control and fibronectin-modified Si-NW array, with only the 20 largest CTF from each group included (n = 20).

GFP–vinculin at the respective FA [13,14], it can be deduced that the sampling of the largest 20 CTF was better at representing the cell's mechanical properties. Although in a single cell, dozens of CTF can be obtained, the sampling of all measurable CTF may not be the optimized indicator to reflect the cells' features. Because the many relatively smaller CTF in a "higher" group may mix up with the relatively "larger CTF" in a "low" group, making the difference vague or even reversed.

It's worthy to mention that we were not doing "cherry-pick" during the data analysis, but followed an honest and understandable standard. Because there have been no established criteria how much CTF should be included for each cell, we tried to find out which data can best represent the most critical feature of a cells' mechanical property. In the first try, we included all the measured CTF to do statistical analysis between the control and Fn groups at each time point. The n varied in each group because for each cell, the number of measurable CTF was different. In this try, we presented all the original data. In the second try, we decreased the number of CTF in each cell for statistical analysis. We wanted to find out what's the situation when only the few largest CTF in each cell were included. The number of measurable CTF in each cell was different, which we believe was a natural state of the cells and shouldn't be interfered. That's why we didn't choose to include the same number of cells and the same number of CTF per cell, but choose to adjust the total number of CTF in each group to be within 102–120. The number of largest CTF varied from 5 to 8 according to the numbers of measurable cells in each group. In the third try, we investigated only the highest 20 CTF in a group, with no regard of the number of CTF per cell.

4. Conclusions

In this study, we reported a high-uniform and precise Si-NW array for CTF measurement. This array had a NW density of 4 μm^{-2}, and the NW had diameters of 267 nm and flat tops. These features were very beneficial for cell culture and CTF measurement. The CTF measured from the fibronectin modified Si-NW array were significantly higher than those measured from the bare Si-NW array from 6 h to 24 h, revealing the importance of this duration for fibronectin to play the modulation role. The enhancement pattern of CTF induced by fibronectin modification was in accordance with that of FA percentage in the entire 36 h culture. Meanwhile, the respective trends of CTF and FA dynamics were also coordinated with each other. In addition, larger CTF quantified from the numerous single Si-NW were found to be better at reflecting a cell's mechanical property. These results identified that the consistency of FA formation and CTF generation lasted for as long as dozens of hours. In addition, the effective modulation slot of the external ECM was within 36 h, revealing the existence of a balanced time

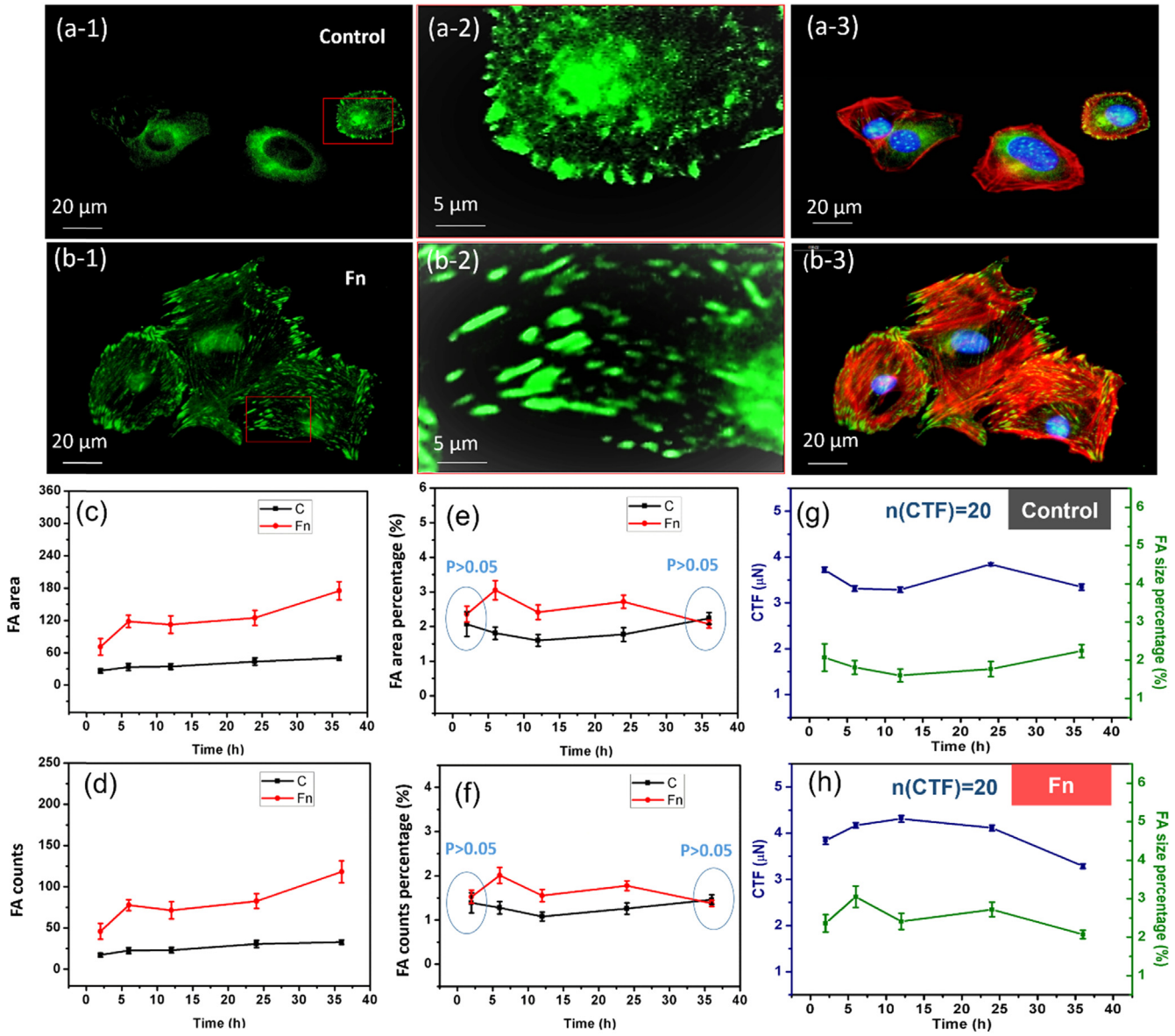

Fig. 5. (a–b) The fluorescent images showing the structures of cells growing on the control and fibronectin-modified Si substrate after 6 h culture: FA (1), enlarged image of a single cell's FA (2), and the merged structures of FA, cytoskeleton F-actin and nucleus (3). (c, d) The measured FA area and FA counts in both Fibronectin and control groups in the 36 h culture, using Image-Pro Plus 6.0 (Average ± SE). (e, f) the analysed results of the FA count percentage (per cell area), and the FA area percentage (per cell area). (g, h) The line-plot showing CTF and FA area percentage dynamics together for the control and fibronectin group respectively.

point for the self-secreted ECM to pull up with the externally added ECM after the cells started to grow on the scaffolds.

To our knowledge, it was up to now one of the few approaches to reach submicron resolution in determining the force field of cells. The merits of high resolution CTF measurement can be analogically regarded as single cell studies such as single cell sequencing. Studying cells at the single-cell level solves the problems of organ or cell community heterogeneity, as well as offers unique opportunities to dissect the interplay between intrinsic cellular processes and extrinsic stimuli [57,58]. Similarly, CTF measurement at high resolution can distinguish CTF at different parts of a single cell and offers unique information about the cellular responses and development. Because of the high density of the NWs, detailed information of the spatial distribution of the CTF was obtained. This not only prevented the cells from sinking to the array bottom, but also allowed the measurement of large amount of CTF. Eventually it became better at detecting the largest CTF, which were more critical to reflect a cell's mechanical property than the ordinary ones. Although the Si-NW array had the shortage of only measuring the periphery of cells, it didn't influence much on the CTF detection. Previous studies using transparent polymer nanopillar array for real-time measurement has demonstrated that the most of the measurable CTF located at the periphery of the cells [59,60]. Also, studies using quartz nanopillar substrates for CTF measurement revealed that the CTF at the edge of the cells were much stronger than those at the centeral part of T cells by exploring the cross-sectional CTF distribution [61]. Therefore our Si-NW array could serve as a superb tool for CTF measurement. This study provided valuable information for the understanding of the CTF derivation dynamics and the design of ECM modified tissue engineering scaffold.

Acknowledgements

This work was supported by the national key R&D project from Minister of Science and Technology, China (2016YFA0202703), National Natural Science Foundation of China (Grant Nos. 31571006, 81601629), Beijing Natural Science Foundation (Grant No. 2182091),

Beijing Talents Fund (20150000021223ZK21) and “Thousands Talents” program for pioneer researcher and his innovation team.

Appendix A. Supporting information

Supplementary data associated with this article can be found in the online version at http://dx.doi.org/10.1016/j.nanoen.2018.05.057.

References

[1] B. Geiger, A. Bershadsky, R. Pankov, K.M. Yamada, Transmembrane extracellular matrix–cytoskeleton crosstalk, Nat. Rev. Mol. Cell Biol. 2 (2001) 793–805, http://dx.doi.org/10.1038/35099066.

[2] G.C. Reilly, A.J. Engler, Intrinsic extracellular matrix properties regulate stem cell differentiation, J. Biomech. 43 (2010) 55–62, http://dx.doi.org/10.1016/j.jbiomech.2009.09.009.

[3] C.M. Lo, H.B. Wang, M. Dembo, Y.L. Wang, Cell movement is guided by the rigidity of the substrate, Biophys. J. 79 (2000) 144–152, http://dx.doi.org/10.1016/S0006-3495(00)76279-5.

[4] M.H. Zaman, L.M. Trapani, A.L. Sieminski, D. Mackellar, H. Gong, R.D. Kamm, A. Wells, D.A. Lauffenburger, P. Matsudaira, Migration of tumor cells in 3D matrices is governed by matrix stiffness along with cell-matrix adhesion and proteolysis, Proc. Natl. Acad. Sci. USA 103 (2006) 10889–10894, http://dx.doi.org/10.1073/Pnas.0606087103.

[5] R. Pankov, K.M. Yamada, Fibronectin at a glance, J. Cell Sci. 115 (2002) 3861–3863, http://dx.doi.org/10.1242/jcs.00059.

[6] Y. Zhu, M.F. Leong, W.F. Ong, M.B. Chan-Park, K.S. Chian, Esophageal epithelium regeneration on fibronectin grafted poly(l-lactide-co-caprolactone) (PLLC) nanofiber scaffold, Biomaterials 28 (2007) 861–868, http://dx.doi.org/10.1016/j.biomaterials.2006.09.051.

[7] L.L. Hench, J.M. Polak, Third-generation biomedical materials, Science (80-.) 295 (2002) 1014–1017, http://dx.doi.org/10.1126/science.1067404.

[8] S.K. Sastry, K. Burridge, Focal adhesions: a nexus for intracellular signaling and cytoskeletal dynamics, Exp. Cell Res. 261 (2000) 25–36, http://dx.doi.org/10.1006/excr.2000.5043.

[9] D.R. Critchley, Focal adhesions - The cytoskeletal connection, Curr. Opin. Cell Biol. 12 (2000) 133–139, http://dx.doi.org/10.1016/S0955-0674(99)00067-8.

[10] D.M. Helfman, E.T. Levy, C. Berthier, M. Shtutman, D. Riveline, I. Grosheva, A. Lachish-Zalait, M. Elbaum, A.D. Bershadsky, Caldesmon inhibits nonmuscle cell contractility and interferes with the formation of focal adhesions, Mol. Biol. Cell 10 (1999) 3097–3112, http://dx.doi.org/10.1167/iovs.12-11575.

[11] J.T. Parsons, K.H. Martin, J.K. Slack, J.M. Taylor, S.A. Weed, Focal adhesion kinase: a regulator of focal adhesion dynamics and cell movement, Oncogene 19 (2000) 5606–5613, http://dx.doi.org/10.1038/sj.onc.1203877.

[12] T. Xie, L. Li, Stem cells and their niche: an inseparable relationship, Development 134 (2007) 2001–2006 〈http://www.ncbi.nlm.nih.gov/entrez/query.fcgi?cmd=Retrieve&db=PubMed&dopt=Citation&list_uids=17507401〉.

[13] R. Mechanism, D. Riveline, E. Zamir, N.Q. Balaban, U.S. Schwarz, T. Ishizaki, S. Narumiya, Z. Kam, B. Geiger, A.D. Bershadsky, focal contacts as mechanosensors: externally applied local mechanical force induces growth of focal contacts by an mDia1-dependent and rock-independent mechanism, J. Cell Biol. 153 (2001) 1175–1185.

[14] N.Q. Balaban, U.S. Schwarz, D. Riveline, P. Goichberg, G. Tzur, I. Sabanay, D. Mahalu, S. Safran, A. Bershadsky, L. Addadi, B. Geiger, Force and focal adhesion assembly: a close relationship studied using elastic micropatterned substrates, Nat. Cell Biol. 3 (2001) 466–472.

[15] B.R. Sarangi, M. Gupta, B.L. Doss, N. Tissot, F. Lam, R.-M. Mège, N. Borghi, B. Ladoux, Coordination between intra- and extracellular forces regulates focal adhesion dynamics, Nano Lett. (2016) 399–406, http://dx.doi.org/10.1021/acs.nanolett.6b04364.

[16] Y. Cai, N. Biais, G. Giannone, M. Tanase, G. Jiang, J.M. Hofman, C.H. Wiggins, P. Silberzan, A. Buguin, B. Ladoux, M.P. Sheetz, Nonmuscle myosin IIA-dependent force inhibits cell spreading and drives F-actin flow, Biophys. J. 91 (2006) 3907–3920, http://dx.doi.org/10.1529/biophysj.106.084806.

[17] S.V. Plotnikov, A.M. Pasapera, B. Sabass, C.M. Waterman, Force fluctuations within focal adhesions mediate ECM-rigidity sensing to guide directed cell migration, Cell 151 (2012) 1513–1527, http://dx.doi.org/10.1016/j.cell.2012.11.034.

[18] V. Maruthamuthu, B. Sabass, U.S. Schwarz, M.L. Gardel, Cell-ECM traction force modulates endogenous tension at cell-cell contacts, Proc. Natl. Acad. Sci. USA 108 (2011) 4708–4713, http://dx.doi.org/10.1073/pnas.1011123108.

[19] M.L. Smith, D. Gourdon, W.C. Little, K.E. Kubow, R.A. Eguiluz, S. Luna-Morris, V. Vogel, Force-induced unfolding of fibronectin in the extracellular matrix of living cells, PLoS Biol. 5 (2007) 2243–2254, http://dx.doi.org/10.1371/journal.pbio.0050268.

[20] C.A. Lemmon, C.S. Chen, L.H. Romer, Cell traction forces direct fibronectin matrix assembly, Biophys. J. 96 (2009) 729–738, http://dx.doi.org/10.1016/j.bpj.2008.10.009.

[21] R. Perez-jimenez, A. Alonso-caballero, R. Berkovich, D. Franco, M. Chen, P. Richard, C.L. Badilla, J.M. Fernandez, Probing the E ff ect of force on HIV - 1 receptor CD4, ACS Nano (2014) 10313–10320.

[22] A. Beaussart, A.E. Baker, S.L. Kuchma, S. El-Kirat-Chatel, G.A. O'Tolle, Y.F. Dufrene, G.A.O. Toole, Nanoscale adhesion forces of pseudomonas aeruginosa type IV Pili, ACS Nano 8 (2014) 10723–10733, http://dx.doi.org/10.1021/nn5044383.

[23] S. El-Kirat-Chatel, A. Beaussart, S. Derclaye, D. Alsteens, S. Kucharikova, P. Van Dijck, Y.F. Dufrene, Force nanoscopy of hydrophobic interactions in the fungal pathogen candida glabrata, ACS Nano 9 (2015) 1648–1655, http://dx.doi.org/10.1021/nn506370f.

[24] M. Unal, Y. Alapan, H. Jia, A.G. Varga, K. Angelino, M. Aslan, I. Sayin, C. Han, Y. Jiang, Z. Zhang, U.A. Gurkan, Micro and nano-scale technologies for cell mechanics, Nanobiomedicine 1 (2014) 1–5, http://dx.doi.org/10.5772/59379.

[25] Kweku A. Addae-Mensah, John P. Wikswo, Measurement techniques for cellular biomechanics in vitro, Exp. Biol. Med. 233 (2008) 792–809, http://dx.doi.org/10.3181/0710-MR-278.Measurement.

[26] M. Benoit, D. Gabriel, G. Gerisch, H.E. Gaub, Discrete interactions in cell adhesion measured by single-molecule force spectroscopy, Nat. Cell Biol. 2 (2000) 313–317.

[27] X. Wang, T. Ha, Defining single molecular forces required to activate integrin and notch signaling, Science (80-.) 7219 (2013) 991–995.

[28] T. Das, T.K. Maiti, S. Chakraborty, Traction force microscopy on-chip: shear deformation of fibroblast cells, Lab. Chip 8 (2008) 1308–1318, http://dx.doi.org/10.1039/b803925a.

[29] U.S. Schwarz, N.Q. Balaban, D. Riveline, A. Bershadsky, B. Geiger, S.A. Safran, Calculation of forces at focal adhesions from elastic substrate data: the effect of localized force and the need for regularization, Biophys. J. 83 (2002) 1380–1394, http://dx.doi.org/10.1016/S0006-3495(02)73909-X.

[30] B. Li, L. Xie, Z.C. Starr, Z. Yang, J. Lin, J.H. Wang, Development of micropost force sensor array with culture experiments for determination of cell traction forces, Cell Motil. Cytoskelet. 64 (2007) 509–518, http://dx.doi.org/10.1002/cm.20200.

[31] J.M. Mann, R.H.W. Lam, S. Weng, Y. Sun, J. Fu, A silicone-based stretchable micropost array membrane for monitoring live-cell subcellular cytoskeletal response, Lab. Chip 12 (2012) 731–740, http://dx.doi.org/10.1039/c2lc20896b.

[32] B.M.T. Yang, N.J. Sniadecki, C.S. Chen, Geometric considerations of micro- to nanoscale elastomeric post arrays to study cellular traction forces, Adv. Mater. 19 (2007) 3119–3123, http://dx.doi.org/10.1002/adma.200701956.

[33] Y. Xiang, D.A. Lavan, Analysis of soft cantilevers as force transducers, Appl. Phys. Lett. 90 (2007) 133901, http://dx.doi.org/10.1063/1.2716376.

[34] K.R. Milner, C.A. Siedlecki, Submicron poly (L -lactic acid) pillars affect fibroblast adhesion and proliferation, J. Biomed. Mater. Res. Part A (2007), http://dx.doi.org/10.1002/jbm.a.

[35] J.H. Wang, J. Lin, Cell traction force and measurement methods, Biomech. Model Mechanobiol. 6 (2007) 361–371, http://dx.doi.org/10.1007/s10237-006-0068-4.

[36] B.E. Mussig, T. Steinberg, S. Schulz, J.P. Spatz, J. Ulmer, N. Grabe, A. Kohl, G. Komposch, P. Tomakidi, Connective-tissue fibroblasts established on micropillar interfaces are pivotal for epithelial-tissue morphogenesis, Adv. Funct. Mater. 18 (2008) 1–11, http://dx.doi.org/10.1002/adfm.200800381.

[37] S. Bonde, N. Buch-månson, K.R. Rostgaard, T.K. Andersen, T. Berthing, K.L. Martinez, Exploring arrays of vertical one-dimensional nanostructures for cellular investigations, Nanotechnology 25 (2014) 362001, http://dx.doi.org/10.1088/0957-4484/25/36/362001.

[38] K.Y. Baik, S.Y. Park, S. Namgung, D. Kim, D. Cho, M. Lee, Synthetic nanowire / nanotube-based solid substrates for controlled cell growth, Nano Converg. 1 (2014) 28, http://dx.doi.org/10.1186/s40580-014-0028-0.

[39] J.F. Zimmerman, G.F. Murray, Y. Wang, J.M. Jumper, J.R. Austin, B. Tian, Free-standing Kinked silicon nanowires for probing inter- and intracellular force dynamics, Nano Lett. 15 (2015) 5492–5498, http://dx.doi.org/10.1021/acs.nanolett.5b01963.

[40] Y. Jin, Y. Zhang, H. Ouyang, Quantification of cell traction force of osteoblast cells using Si nanopillar-based mechanical sensor, Sens. Mater. 27 (2015) 1071–1077, http://dx.doi.org/10.18494/SAM.2015.1144.

[41] B.Z. Huang, H. Fang, J. Zhu, Fabrication of silicon nanowire arrays with controlled diameter, length, and density, Adv. Mater. 19 (2007) 744–748.

[42] J. Cai, L. Qi, Recent advances in antireflective surfaces based on nanostructure arrays, Mater. Horiz. 2 (2015) 37–53, http://dx.doi.org/10.1039/C4MH00140K.

[43] F. Patolsky, B.P. Timko, G. Yu, Y. Fang, A.B. Greytak, G. Zheng, C.M. Lieber, Detection, stimulation, and inhibition of neuronal signals with high-density nanowire transistor arrays, Science (80-.) 313 (2006) 1100–1105.

[44] Y. Cui, Q. Wei, H. Park, C.M. Lieber, Nanowire nanosensors for highly sensitive and selective detection of biological and chemical species, Science (80-.) 293 (2001) 1289–1293.

[45] Z. Li, J. Song, G. Mantini, M.Y. Lu, H. Fang, C. Falconi, L.J. Chen, Z.L. Wang, Quantifying the traction force of a single cell by aligned silicon nanowire array, Nano Lett. 9 (2009) 3575–3580, http://dx.doi.org/10.1021/nl901774m.

[46] P.K. Sahoo, R. Janissen, M.P. Monteiro, A. Cavalli, D.M. Murillo, M.V. Merfa, C.L. Cesar, H.F. Carvalho, A.A. De Souza, E.P.A.M. Bakkers, M.A. Cotta, Nanowire arrays as cell force sensors to investigate adhesin-enhanced holdfast of single cell bacteria and biofilm stability, Nano Lett. 16 (2016) 4656–4664, http://dx.doi.org/10.1021/acs.nanolett.6b01998.

[47] K. Adolfsson, H. Persson, J. Wallentin, S. Oredsson, L. Samuelson, J.O. Tegenfeldt, M.T. Borgstro, C.N. Prinz, Fluorescent nanowire heterostructures as a versatile tool for biology applications, Nano Lett. 13 (2013) 4728–4732.

[48] M. Lexholm, D.B. Suyatin, G. Hammarin, D. Hessman, L. Samuelson, L. Montelius, M. Kanje, C.N. Prinz, Fifteen-Piconewton force detection from neural growth cones using nanowire arrays, Nano Lett. 10 (2010) 782–787, http://dx.doi.org/10.1021/nl902675h.

[49] S.Y. Kim, E.G. Yang, Collective behaviors of mammalian cells on amine-coated silicon nanowires, Nanotechnology 455704 (2013), http://dx.doi.org/10.1088/0957-4484/24/45/455704.

[50] W. Kim, J.K. Ng, M.E. Kunitake, B.R. Conklin, P. Yang, Interfacing silicon nanowires with mammalian cells, J. Am. Chem. Soc. 129 (2007) 7228–7229.

[51] N. Buch-Månson, S. Bonde, J. Bolinsson, T. Berthing, J. Nygård, K.L. Martinez,

Towards a better prediction of cell settling on nanostructure arrays - simple means to complicated ends, Adv. Funct. Mater. 25 (2015) 3246–3255, http://dx.doi.org/10.1002/adfm.201500399.
[52] H. Persson, C. Købler, K. Mølhave, L. Samuelson, J.O. Tegenfeldt, S. Oredsson, C.N. Prinz, Fibroblasts cultured on nanowires exhibit low motility, impaired cell division, and DNA damage, Small 9 (2013) 4006–4016, http://dx.doi.org/10.1002/smll.201300644.
[53] R. Elnathan, M. Kwiat, F. Patolsky, N.H. Voelcker, Engineering vertically aligned semiconductor nanowire arrays for applications in the life sciences, Nano Today 9 (2014) 172–196, http://dx.doi.org/10.1016/j.nantod.2014.04.001.
[54] H. Persson, Z. Li, J.O. Tegenfeldt, S. Oredsson, C.N. Prinz, From immobilized cells to motile cells on a bed-of-nails: effects of vertical nanowire array density on cell behaviour, Sci. Rep. 5 (2016) 18535, http://dx.doi.org/10.1038/srep18535.
[55] R.L. Wasserstein, N.A. Lazar, The ASA's statement on *p* -values: context, process, and purpose, Am. Stat. 70 (2016) 129–133, http://dx.doi.org/10.1080/00031305.2016.1154108.
[56] C.S. Chen, M. Mrksich, S. Huang, G.M. Whitesides, D.E. Ingber, Geometric control of cell life and death, Science (80-.) 276 (1997) 1425–1428.
[57] A.E. Saliba, A.J. Westermann, S.A. Gorski, J. Vogel, Single-cell RNA-seq: advances and future challenges, Nucleic Acids Res. 42 (2014) 8845–8860, http://dx.doi.org/10.1093/nar/gku555.
[58] J. Liang, W. Cai, Z. Sun, Single-cell sequencing technologies: current and future, J. Genet. Genom. 41 (2014) 513–528, http://dx.doi.org/10.1016/j.jgg.2014.09.005.
[59] F. Margadant, Adaptive rheology and ordering of cell cytoskeleton govern matrix rigidity sensing, Nat. Commun. 6 (2015) 7525, http://dx.doi.org/10.1038/ncomms8525.
[60] O. Roure, A. Saez, A. Buguin, R.H. Austin, P. Chavrier, P. Siberzan, B. Ladoux, Force mapping in epithelial cell migration, Proc. Natl. Acad. Sci. USA 102 (2005) 2390–2395.
[61] D. Kim, G. Kim, J. Hyung, W. Lee, C. Hong, S. Lee, Direct observation of CD4 T cell morphologies and their cross-sectional traction force derivation on quartz nano-pillar substrates using focused ion beam technique Direct observation of CD4 T cell morphologies and their cross-sectional traction force deriv, Nanoscale Res. Lett. 8 (2013) 322.